Electronic Supplementary Material (ESI) for Physical Chemistry Chemical Physics.

Supporting Info: Simulating the Solvation Structure of Low- and High-Spin $[Fe(bpy)_3]^{2+}$: Long-Range Dispersion and Many-Body Effects

Habiburrahman Zulfikri,[†,‖] Mátyas Pápai,[‡,¶] and Asmus Ougaard Dohn[*,†,§]

†*Science Institute and Faculty of Physical Sciences, VR-III, University of Iceland, Reykjavík, Iceland*

‡*Wigner Research Centre for Physics, P.O. Box 49, H-1525 Budapest, Hungary.*

¶*Department of Chemistry, Technical University of Denmark, Kemitorvet 207, DK-2800 Kongens Lyngby, Denmark.*

§*Department of Physics, Technical University of Denmark*

‖*Present Address: Department of Chemical Engineering, Faculty of Engineering, Universitas Indonesia, Depok 16424, Indonesia*

E-mail: asod@hi.is

Contents

S1 Model System Basis Set Benchmarks **S3**

S1.1 Density functional theory calculations S3

S1.2 DLPNO-CCSD(T) calculations S6

S1.3 DFT and DLPNO-CCSD(T) calculations for the CAC multimer model $[Fe(py)2]^{2+}$ $2H_2O\cdots H_2O$ S7

S2 $[Fe(bpy)_3]^{2+}\cdots nH_2O$ (n = 3,4) Interaction Energies **S9**

S3 CP2K BSSE Analysis **S11**

S4 Water-shell RMSD Comparisons **S12**

S5 Further MM Calculations and Details **S13**

S5.1 Multimer Interaction Energy Curves S13

S5.2 Additional MD Studies S14

S5.3 MM Solvent and Counterions S15

S5.4 CPCM Effects on Partial Charges S17

S5.5 Relationship between the 20-water cluster and the liquid-phase avg. shell . . S21

S5.6 LJ Parameters S22

S6 Further ΔV_{CS} and ΔV_{WW} Calculations **S22**

S6.1 BSSE Estimation of ΔV_{CS} and ΔV_{WW} S23

S7 Further Many-Body Calculations **S25**

References **S26**

S1 Model System Basis Set Benchmarks

To allow affordably establishing computational ingredients for computing the interaction energy using different methods, we created a model system consisting of a metal center ion, two pyridine ligands and a water molecule noncovalently bound to the ion as shown in Figure S1. The resulting $[Fe(py)_2]^{2+} \cdots H_2O$ model retains the same noncovalent interaction as in $[Fe(bpy)_3]^{2+} \cdots H_2O$. The geometry of the model was built by deleting four pyridine moieties from the B3LYP-D3(BJ)/def2-TZVP optimized geometry of the $[Fe(bpy)_3]^{2+} \cdots H_2O$ bimolecular system, and capping each dangling bond with a hydrogen atom at a distance of 1.032 Å from the carbon atom. The study conducted here deals with a system in LS state, the water molecule in pose A, and a Fe−O distance of 4.5 Å representing a geometry in the vicinity of the minimum of the potential energy curve.

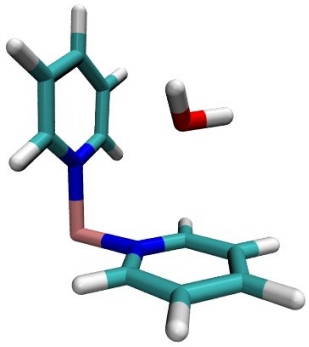

Figure S1: $[Fe(py)_2]^{2+} \cdots H_2O$ bimolecular system employed in the basis-set convergence study of the interaction energy.

S1.1 Density functional theory calculations

We first examine the effect of including the relativistic correction in the framework of Douglas−Kroll−Hess (DKH) to the DFT-D3(BJ) interaction energy and showed the results in Table S1. In general, the DKH method lowers the interaction energy by no more than 0.01 eV. As the improvement is very small, further calculations will not employ relativistic treatment. Next, we investigated the effect of using different sizes of DFT integration

grid to the interaction energy. Here, the multigrid scheme, which is denoted as grid(m,n) where m and n indicate the grid size as defined in ORCA for SCF iteration and final energy evaluation, respectively, is employed. Calculations with grid(2,4) and grid(4,6) setting result in negligible changes to the interaction energy as shown also in Table S1. Hence, the default setting in ORCA, i.e., Grid(2,4), is sufficiently accurate for interaction-energy studies.

Table S1: Non-relativistic and Douglas−Kroll−Hess (DKH) Relativistic DFT-D3(BJ) CP-corrected interaction energy in eV of the LS state of $[Fe(py)_2]^{2+} \cdots H_2O$ in pose A at a Fe−O distance of 4.5 Å.

Functional	Basis set	Non-relativistic		Relativistic	
		Grid(2,4)	Grid(4,6)	Grid(2,4)	Grid(4,6)
BLYP	def2-SVP	−0.506	−0.506	−0.511	−0.511
	def2-TZVP	−0.466	−0.457	−0.466	−0.466
	def2-QZVPP	−0.436	−0.430	−0.436	−0.436
	ma-def2-SVP	−0.451	−0.447	−0.449	−0.449
	ma-def2-TZVP	−0.438	−0.438	−0.438	−0.438
	ma-def2-QZVPP	−0.430	−0.425	−0.430	−0.430
B3LYP	def2-SVP	−0.470	−0.470	−0.476	−0.476
	def2-TZVP	−0.459	−0.459	−0.458	−0.458
	def2-QZVPP	−0.434	−0.434	−0.434	−0.434
	ma-def2-SVP	−0.456	−0.456	−0.458	−0.458
	ma-def2-TZVP	−0.438	−0.438	−0.438	−0.438
	ma-def2-QZVPP	−0.430	−0.430	−0.430	−0.430
B2PLYP	def2-SVP	−0.437	−0.437	−0.444	−0.444
	def2-TZVP	−0.444	−0.445	−0.444	−0.444
	def2-QZVPP	−0.429	−0.429	−0.428	−0.428
	ma-def2-SVP	−0.436	−0.436	−0.439	−0.440
	ma-def2-TZVP	−0.434	−0.427	−0.426	−0.427
	ma-def2-QZVPP	−0.425	−0.426	−0.425	−0.425

Having shown that the non-relativistic calculations in combination with the default grid settings in ORCA give results with an error below 0.01 eV for the three DFT functionals, we continue to the basis-set convergence study of the interaction energy using the def2 basis-set family and the corresponding minimally augmented version. We regard the CP-corrected interaction energy acquired with ma-def2-QZVP basis set as the reference values for each functional. As shown in Table S2, both def2-QZVP and ma-def2-TZVP obtain CP-corrected interaction energies within 0.01 eV of the reference values. Since the latter basis set contain

less than a half of the number of basis functions than the former, we proceed our interaction energy study with the latter (ma-def2-TZVP) basis set.

Table S2: DFT and DFT-D3(BJ) interaction energies in eV of the LS state of $[Fe(py)_2]^{2+} \cdots H_2O$ in pose A at a Fe−O distance of 4.5 Å. The values we choose as references for each functional is colored in blue

Functional	Basis set	Uncorrected		CP-corrected		E_{BSSE}
		DFT	DFT-D3(BJ)	DFT	DFT-D3(BJ)	
BLYP	def2-SVP	−0.518	−0.689	−0.335	−0.506	−0.183
	def2-TZVP	−0.344	−0.515	−0.295	−0.466	−0.049
	def2-QZVP	−0.284	−0.455	−0.266	−0.436	−0.019
	ma-def2-SVP	−0.369	−0.540	−0.281	−0.451	−0.089
	ma-def2-TZVP	−0.310	−0.481	−0.267	−0.438	−0.043
	ma-def2-QZVP	−0.267	−0.437	−0.260	−0.430	−0.007
B3LYP	def2-SVP	−0.484	−0.628	−0.327	−0.470	−0.158
	def2-TZVP	−0.355	−0.499	−0.315	−0.459	−0.040
	def2-QZVP	−0.304	−0.448	−0.290	−0.434	−0.014
	ma-def2-SVP	−0.391	−0.535	−0.312	−0.456	−0.079
	ma-def2-TZVP	−0.334	−0.478	−0.294	−0.438	−0.040
	ma-def2-QZVP	−0.292	−0.436	−0.286	−0.430	−0.006
B2PLYP	def2-SVP	−0.521	−0.595	−0.364	−0.437	−0.158
	def2-TZVP	−0.420	−0.493	−0.371	−0.444	−0.049
	def2-QZVP	−0.373	−0.446	−0.355	−0.429	−0.018
	ma-def2-SVP	−0.480	−0.553	−0.363	−0.436	−0.117
	ma-def2-TZVP	−0.411	−0.485	−0.361	−0.434	−0.050
	ma-def2-QZVP	−0.363	−0.437	−0.352	−0.425	−0.011

In Table S3, we show that the self-consistent and non self-consistent computation of the non-local dispersion correction yield essentially the same results (within 0.003 eV). Therefore, the results of the computationally inexpensive non self-consistent DFT-NL computation is the ones shown in the manuscript.

Table S3: Comparison between the uncorrected (UC) and Counterpoise-corrected (CP) LS state interaction energies of $[Fe(bpy)_3]^{2+}$ and H_2O (eV) obtained from different treatment of dispersion within DFT-NL framework at a fixed Fe−O distance of 4.50 Å.

Method	UC	CP
BLYP/def2-TZVP		
non self-consistent NL	−0.488	−0.537
self-consistent NL	−0.491	−0.540
B3LYP/def2-TZVP		
non self-consistent NL	−0.469	−0.508
self-consistent NL	−0.470	−0.510

S1.2 DLPNO-CCSD(T) calculations

Table S4: DLPNO-CCSD(T) interaction energy in eV of the LS state of $[Fe(py)_2]^{2+} \cdots H_2O$ in pose A at a Fe−O distance of 4.5 Å.

Basis set	Uncorrected	CP-corrected	E_{BSSE}
	`NormalPNO`		
def2-SVP	−0.546	−0.393	−0.154
def2-TZVP	−0.490	−0.426	−0.064
def2-QZVP	−0.451	−0.443	−0.008
ma-def2-SVP	−0.609	−0.412	−0.197
ma-def2-TZVP	−0.510	−0.421	−0.090
ma-def2-QZVP	−0.449	−0.423	−0.026
	`TightPNO`		
def2-SVP	−0.544	−0.386	−0.158
def2-TZVP	−0.480	−0.415	−0.065
def2-QZVP	−0.442	−0.434	−0.009
ma-def2-SVP	−0.609	−0.410	−0.199
ma-def2-TZVP	−0.495	−0.405	−0.090
ma-def2-QZVP	−0.439	−0.410	−0.029

Table S4 shows DLPNO-CCSD(T) interaction energy using def2 and ma-def2 series of basis set. We first notice that the basis-set superposition error is larger in ma-def2-QZVP than in def2-QZVP calculations, and hence, the results obtained from the def2-QZVP calculations serve as the reference. Secondly, the cheaper `NormalPNO` settings of the DLPNO-CCSD(T) method result in slightly lower def2-QZVP interaction energy than that of the `TightPNO` settings by 0.009 eV. Finally, the def2-TZVP calculations slightly overbind by 0.017 eV, as

compared to the calculations using the def2-QZVP basis set. Since a combination of loosening the PNO threshold from TightPNO to NormalPNO and reducing the basis set size from def2-QZVP to def2-TZVP presents a combination of parameters that only give a binding energy that is higher by 0.008 eV from the reference, we will employ this recipe for computing the DLPNO-CCSD(T) interaction energy of the larger $[Fe(bpy)_3]^{2+} \cdots n H_2O$ system.

S1.3 DFT and DLPNO-CCSD(T) calculations for the CAC multimer model $[Fe(py)2]^{2+}$ $2H_2O \cdots H_2O$

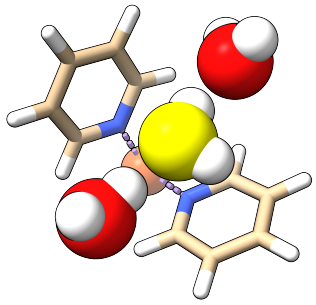

Figure S2: The $[Fe(py)2]^{2+}$ $2H_2O \cdots H_2O$ model system with water in the CAC arrangement used in the basis-set convergence study of multimer interaction energies.

In aqueous environment, a water (solvent) molecule is interacting noncovalently with other water molecules via hydrogen bonds in addition to with a complex. In this subsection, we investigate interaction energy of a water molecule hydrogen-bonded with two other water molecules and noncovalently interacted with one cation model complex consisting of an Iron(II) center and two pyridine ligands (see Figure S2).

We here benchmark the dispersion-corrected B3LYP-D3(BJ) and uncorrected B3LYP interaction energies against DLPNO-CCSD(T) for the model $[Fe(py)2]^{2+}$ $2H_2O \cdots H_2O$ in the multimer arrangement CAC (the $\cdots H_2O$ molecule is in pose A). As for the dimer model $[Fe(py)2]^{2+} \cdots H_2O$, we consider the LS state with a Fe-O distance of 4.5 Å (for the water molecule in pose A). The geometry was constructed the same way as for the dimer, i.e., by

Table S5: DFT and DLPNO-CCSD(T) interaction energies in eV of the LS state of $[Fe(py)_2]^{2+}$ $2H_2O\cdots H_2O$ in pose A at a Fe−O distance of 4.5 Å.

Basis set	Uncorrected	CP-corrected	E_{BSSE}
B3LYP			
def2-SVP	−0.773	−0.417	−0.356
def2-TZVP	−0.457	−0.378	−0.079
def2-QZVP	−0.378	**−0.355**	−0.022
ma-def2-SVP	−0.511	−0.386	−0.125
ma-def2-TZVP	−0.417	−0.363	−0.053
ma-def2-QZVP	−0.362	**−0.354**	−0.008
B3LYP-D3(BJ)			
def2-SVP	−1.004	−0.647	−0.356
def2-TZVP	−0.688	−0.608	−0.079
def2-QZVP	−0.608	**−0.586**	−0.022
ma-def2-SVP	−0.742	−0.617	−0.125
ma-def2-TZVP	−0.647	−0.594	−0.053
ma-def2-QZVP	−0.592	**−0.584**	−0.008
DLPNO-CCSD(T) `NormalPNO`			
def2-SVP	−0.774	−0.405	−0.369
def2-TZVP	−0.613	−0.479	−0.134
def2-QZVP	−0.575	**−0.531**	−0.045
ma-def2-SVP	−0.738	−0.427	−0.311
ma-def2-TZVP	−0.613	−0.469	−0.144
ma-def2-QZVP	−0.582	**−0.539**	−0.043
DLPNO-CCSD(T) `TightPNO`			
def2-SVP	−0.779	−0.404	−0.375
def2-TZVP	−0.602	−0.465	−0.137
def2-QZVP	−0.571	**−0.522**	−0.048
ma-def2-SVP	−0.754	−0.430	−0.324
ma-def2-TZVP	−0.608	−0.460	−0.149
ma-def2-QZVP	−0.570	**−0.528**	−0.042

deleting four pyridine units from the corresponding B3LYP-D3(BJ)/def2-TZVP optimized geometry of $[Fe(py)2]^{2+}$ $2H_2O\cdots H_2O$ in CAC arrangement.

The results of DFT and DLPNO-CCSD(T) calculations using different basis sets and settings are shown in Table S5. As expected, the DFT-calculated CP-corrected interaction energies show convergence with respect to the applied basis set. For DLPNO-CCSD(T), however, the convergence is rather slow, significantly slower than for DLPNO-CCSD(T) for the model dimer, see Table S4. This means that in contrast to the dimer, for the CAC

multimer, an accurate DLPNO-CCSD(T) calculation with a large enough basis set is not feasible. However, the trends seen in Table S4 reveal that the B3LYP-D3(BJ) calculated CP-corrected interaction energy is expected to agree rather well with a converged DLPNO-CCSD(T) result, while the dispersion-uncorrected B3LYP method severely underestimates the interaction energy.

S2 $[Fe(bpy)_3]^{2+} \cdots nH_2O$ (n = 3,4) Interaction Energies

In Table S6, we show the comparison of different dispersion correction treatment in obtaining the position of the minimum in the potential energy curve. The general trend of V_{min} is DFT-NL $\leq$ DFT-D4 $\leq$ DFT-D3(BJ) $<$ DFT.

Table S6: Fe−O strongest-binding distance,R_{min}, in Å and the minimum interaction energy (V_{min}) in eV of the CP-corrected potential energy curve of $[Fe(bpy)_3]^{2+}nH_2O\cdots H_2O$ (n = 2, 3). *The BLYP Pose DBBB calculations did not converge.

Method	Pose CAC				Pose CBD			
	LS		HS		LS		HS	
	R_{min}	V_{min}	R_{min}	V_{min}	R_{min}	V_{min}	R_{min}	V_{min}
BLYP	4.8	−0.301	4.7	−0.402	5.4	−0.428	5.5	−0.464
B3LYP	4.8	−0.363	4.7	−0.443	5.4	−0.489	5.5	−0.510
B2PLYP	4.7	−0.436	4.6	−0.508	5.3	−0.547	5.5	−0.566
BLYP-D3(BJ)	4.6	−0.560	4.5	−0.626	5.3	−0.615	5.5	−0.641
B3LYP-D3(BJ)	4.6	−0.585	4.5	−0.634	5.3	−0.652	5.4	−0.663
B2PLYP-D3(BJ)	4.6	−0.549	4.5	−0.606	5.3	−0.628	5.4	−0.641
BLYP-D4	4.6	−0.556	4.5	−0.632	5.3	−0.618	5.5	−0.620
B3LYP-D4	4.6	−0.576	4.5	−0.634	5.3	−0.646	5.4	−0.657
B2PLYP-D4	4.6	−0.545	4.5	−0.607	5.3	−0.627	5.4	−0.640
BLYP-NL	4.6	−0.608	4.5	−0.678	5.3	−0.669	5.4	−0.680
B3LYP-NL	4.6	−0.612	4.5	−0.665	5.3	−0.684	5.4	−0.695
B2PLYP-NL	4.6	−0.573	4.5	−0.632	5.3	−0.652	5.4	−0.664
OPLS	4.6	−0.596	4.4	−0.678	5.4	−0.596	5.4	−0.628
Method	Pose ACB				Pose DBBB			
	LS		HS		LS		HS	
	R_{min}	V_{min}	R_{min}	V_{min}	R_{min}	V_{min}	R_{min}	V_{min}
BLYP	5.3	−0.367	5.1	−0.356	*			
B3LYP	5.2	−0.423	4.8	−0.411	4.8	−0.512	5.0	−0.541
B2PLYP	5.1	−0.483	4.8	−0.474	4.8	−0.586	4.9	−0.611
BLYP-D3(BJ)	5.1	−0.563	4.6	−0.568	*			
B3LYP-D3(BJ)	5.0	−0.593	4.7	−0.597	4.7	−0.742	4.9	−0.762
B2PLYP-D3(BJ)	5.1	−0.566	4.7	−0.568	4.7	−0.699	4.9	−0.718
BLYP-D4	5.0	−0.565	4.6	−0.578	*			
B3LYP-D4	5.0	−0.590	4.7	−0.596	4.7	−0.725	4.9	−0.743
B2PLYP-D4	5.1	−0.566	4.7	−0.569	4.7	−0.693	4.9	−0.711
BLYP-NL	5.0	−0.614	4.7	−0.623	*			
B3LYP-NL	5.0	−0.625	4.7	−0.631	4.7	−0.781	4.8	−0.806
B2PLYP-NL	5.0	−0.592	4.7	−0.595	4.7	−0.729	4.9	−0.748
OPLS	5.0	−0.674	4.7	−0.654	4.8	−0.766	4.9	−0.807

S3 CP2K BSSE Analysis

The CP2K package[1] is widely used in performing full *ab-initio* molecular dynamics simulations of transition metal complexes in solution phase. Here, we assess the basis-set convergence and BSSE-behavior of the complex-shell interaction energy of the $[Fe(bpy)_3]^{2+} \cdots 17H_2O$ system using the same B3LYP-D3(BJ)/def2-TZVP optimized geometry as used in the other parts of this work. Three basis sets of increasing quality, i.e., DZVP, TZVP and TZV2P, were investigated. DFT Calculations employed a mixed Gaussian and plane waves approach[2] implemented in the CP2K program version 5.1.[3] Goedecker-Teter-Hutter pseudopotentials[4–6] were utilized to describe core electrons of the atoms. The valence states were described with the Gaussian-type MOLOPT basis set with less diffuse primitives from the CP2K package.[7] As the system has no periodicity in all three cartesian directions, the Martyna-Tuckerman scheme[8] for treating the long range interactions is incorporated. A planewave cutoff of 800 Ry and a relative density cutoff of 50 Ry were used.

The complex−shell interaction energies and the corresponding BSSE are shown in Table S7. The percentage of E_{BSSE} is computed with respect to the CP values. Our computations reveal that the most expensive TZV2P complex−shell interaction energy contains about 5% of BSSE. The commonly employed DZVP basis set in AIMD simulations[9] yield larger BSSE (about 10%). This could potentially translate into a tighter and thus more structured solvation shell.

Table S7: CP2K BLYP-D3(BJ) complex−shell interaction energies V_{CS} in eV of the $[Fe(bpy)_3]^{2+} \cdots 17H_2O$ system using the B3LYP-D3(BJ)/def2-TZVP geometry

Basis	LS			HS		
set	UC	CP	E_{BSSE}	UC	CP	E_{BSSE}
DZVP	−2.557	−2.285	−0.272 (10.6%)	−2.548	−2.287	−0.261 (10.2%)
TZVP	−2.371	−2.239	−0.132 (5.6%)	−2.369	−2.240	−0.129 (5.4%)
TZV2P	−2.370	−2.256	−0.114 (4.8%)	−2.383	−2.258	−0.125 (5.2%)

S4 Water-shell RMSD Comparisons

Table S8: RMSD-values in Å between the BLYP-D3(BJ)/def2-TZVP and B3LYP-D3(BJ)/def2-TZVP geometries of $[Fe(bpy)_3]^{2+} \cdots n H_2O$ system, relaxed in ORCA.

	LS				HS			
nH_2O	17	18	19	20	17	18	19	20
RMSD	0.0621	0.0838	0.1176	0.0810	0.2670	0.0862	0.0480	0.0712

Averaging all the RMSDs in table S8 gives a value of 0.1 Å, or around half of the average RMSD between the LS and HS geometries obtained with either functional. The coordinates of the relaxed BLYP geometries can be found online at `https://gitlab.com/asod/febpy3_solvation`.

S5 Further MM Calculations and Details

S5.1 Multimer Interaction Energy Curves

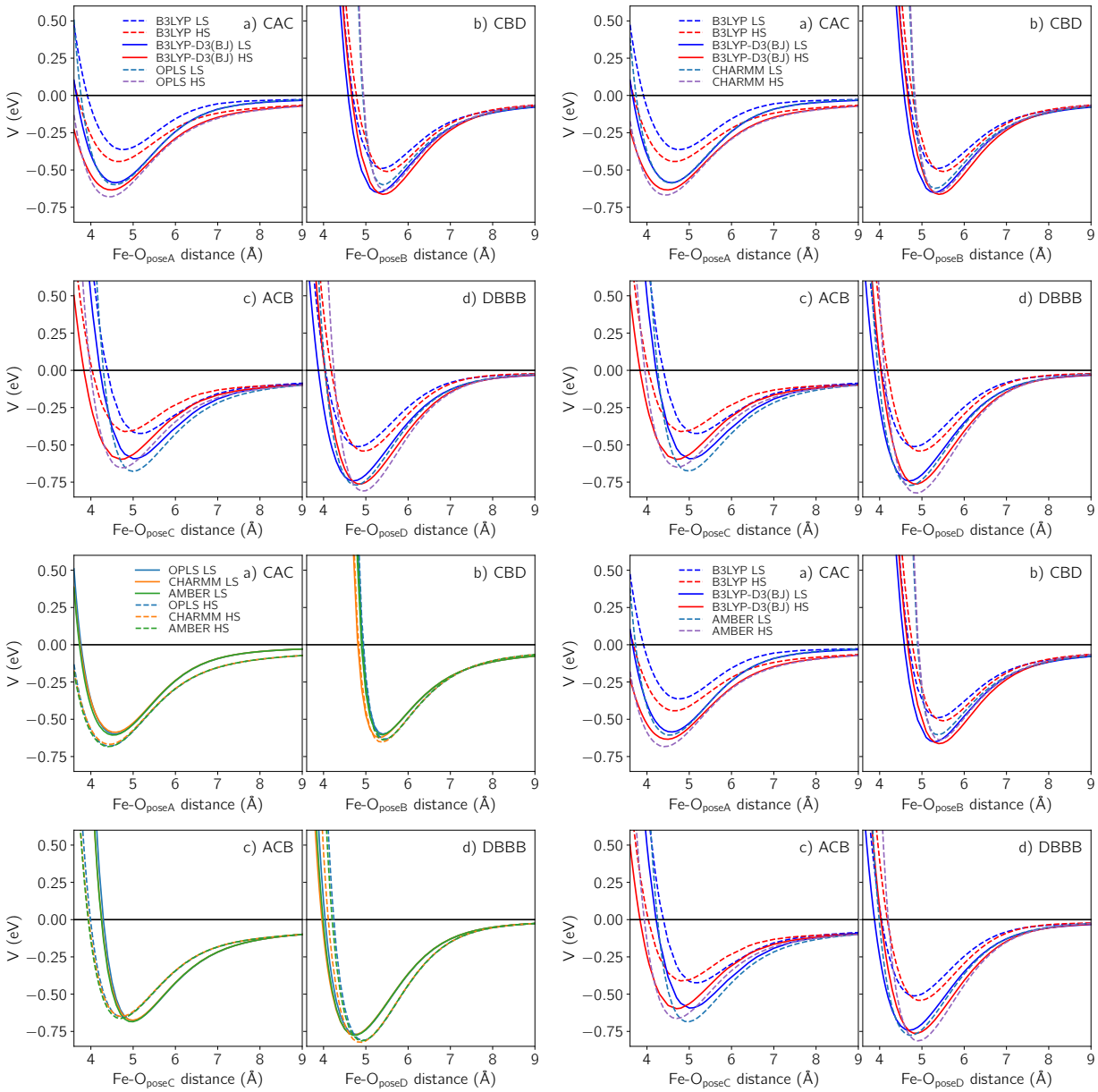

Figure S3: Multimer interaction energy curves, in quadrants of 4, starting top left and going clockwise: OPLS, CHARMM, AMBER, and a comparison of all 3 FFs. The differences are very small, but again, as in fig. 4 in the main text, largest when pose B is directly being scanned.

S5.2 Additional MD Studies

Since the MM parametrization scheme used has only been developed for ground state parametrizations,[10] the simulations carried out and analyzed in this section is solely concerned with the LS state. The top plots in figure S4 shows the effects on the Fe-O and C-O

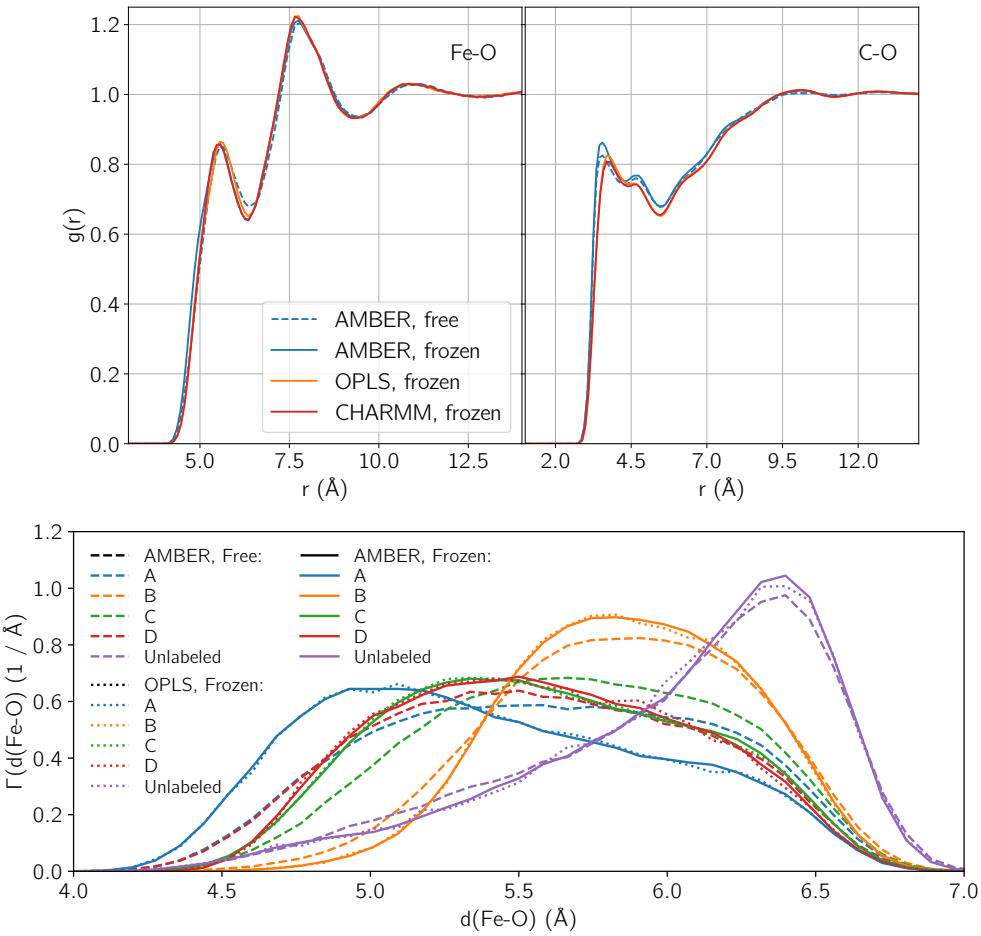

Figure S4: Top: RDFs from simulations using the three FFs of the complex in the LS state. Top left Fe-O, top right: C-O. The 'frozen' RDFs are sampled from trajectories where the geometry has been restrained to its B3LYPD3(BJ) geometry. Bottom: Histograms of the Fe-O distances of the 4 poses in the inner shell, sampled from trajectories run with AMBER and no restraints ('free'), as well as two 'frozen' runs, where the complex has been restrained to its B3LYPD3(BJ)-optimized geometry using 500 kj/mol·Å^2 positional restraints.

RDFs of (i) restraining the complex to its DFT-optimized geometry, and (ii) choice of force field. For the Fe-O RDF, the effects of either are minimal, with the largest change being the first minimum of the RDF being slightly more shallow in the case of the free complex.

For the C-O RDF, the changes are generally small, the largest being brought about by the flexible molecule causing a slight decrease in amplitude of the first peak.

Performing the Linear Sum Assignment-based (LSA) classification of poses and sampling their Fe-O distances shows that restraining the complex pushes the pose C- and especially pose A-distribution towards shorter Fe-O distances, consistent with the slightly faster rise of the Fe-O RDF. Otherwise, the water-shell structure remains largely unchanged by the choice of MM FF, and by whether or not the complex geometry is restrained to the B3LYP-D3(BJ) optimized geometry.

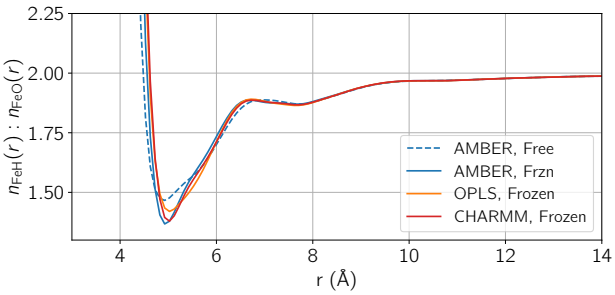

Figure S5: Ratios between the Fe-H and Fe-O running coordination numbers, indicating the preferred orientation of the waters toward the Fe center. Since water has two hydrogens per oxygen, the water is randomly oriented when this ratio is 2.

Figure S5 compares the running coordination numbers between the four models tested in this section. Once more, the changes are very small, with the main difference being between the minimum of the frozen and free AMBER runs, showing that restraining the complex leads to a deepening of the minimum within the first solvation shell. It makes sense that when the complex is allowed to freely move its pyridine ligands, the resulting water-orientation will be less defined.

S5.3 MM Solvent and Counterions

The influence of ion-pairing on the solvation of $[Fe(bpy)_3]^{2+}$ has been discussed in the literature, where one of the latest studies argue that the existence of ion pairing would influence the ground state recovery kinetics of the excited complex.[11] The authors report that no

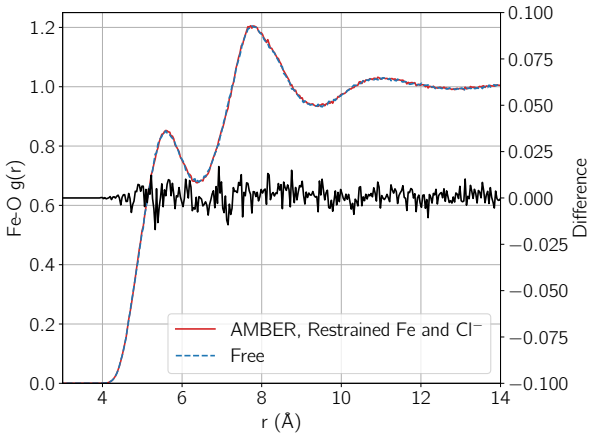

Figure S6: Comparison of the Fe-O RDF between two runs using our AMBER-parametrization. Red curve: RDF sampled from an MD run where positional restraints were applied on the Fe and Cl^--ion positions. Blue dashed curve: RDF sampled from a run without restraints altogether.

such effect is observed, but will not rule out the possibility of (weak) ion pairing taking place entirely.[11] Figure S6 compares the Fe-O RDFs of an MD run where the counterions cannot ion-pair with the complex (red curve), and another MD run where both counterions and complex can diffuse freely, and can thus in principle form ion-pairs. The changes in the RDFs seen in fig. 8 in the main text from removing the counterions have disappeared, indicating that the MM model predicts no significant ion-pairing taking place.

Figure S7 (left) compares the experimental[12] water O-O RDFs with the one obtained us-

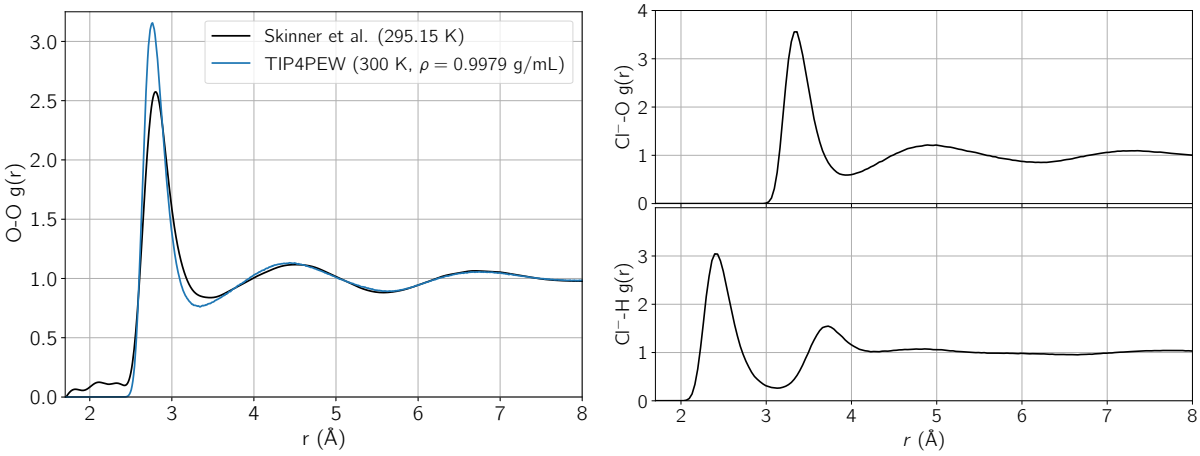

Figure S7: Left: Water O-O RDFs. Black: Experimental,[12] blue: TIP4PEW used in this work, red: BLYP-D3.[9] Right: The counterion-water RDFs.

ing the MM water potential used in this work. The observed over-structuring in the MM MD RDF can be partly attributed to neglecting nuclear quantum effects in performing the dynamics.[13] The right side of the figure shows the RDFs sampled from the counterion to the oxygens (top) and hydrogens (bottom) of water, respectively. As expected, the partially positive charged hydrogens will point inward towards the negative counterion.

S5.4 CPCM Effects on Partial Charges

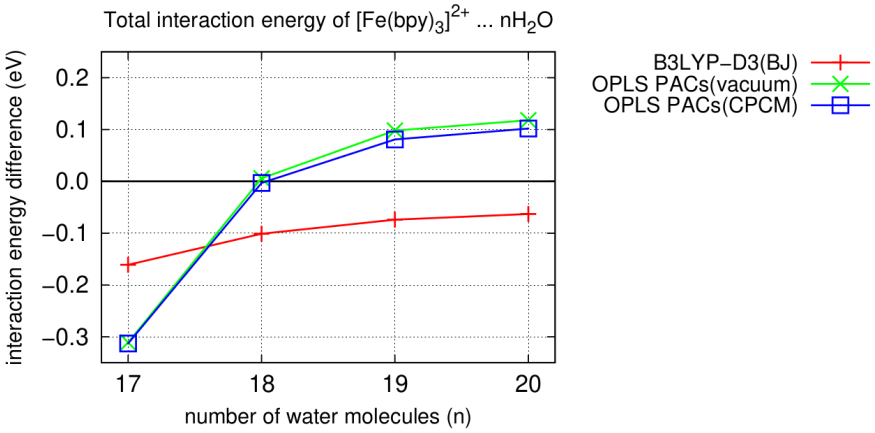

Figure S8: Difference (HS−LS) of the total interaction energies of the $[Fe(bpy)_3]^{2+} \cdots nH_2O$ (n = 17, 18, 19, 20) at the B3LYP-D3(BJ)/def2-TZVP geometries.

In Table S9 we show the partial atomic charges of $[Fe(bpy)_3]^{2+}$ in its HS and LS states obtained from B3LYP-D3(BJ) calculations in vacuum and the CPCM implicit model for water. The total charge of each ligand is also computed to gauge the effect of the solvent on how the charges are distributed. While, in the LS state, polarization from the solvent has negligible effect on the partial atomic charges (PACs) of the complex, the charges were distributed differently in the HS state: When CPCM is used, the PAC of Fe^{2+} becomes more negative by ∼0.3e, while the charge of each ligand becomes more positive by ∼0.1e. We then compare the two sets of charges in computing the HS−LS difference of the total interaction energy in the $[Fe(bpy)_3]^{2+} \cdots nH_2O$ system (n=17,18,19,20). As depicted in Figure S8, the HS-LS OPLS/TIP4PEW interaction energy differences using PACs obtained from calculations in the gas phase and CPCM solvent model are very similar, although the

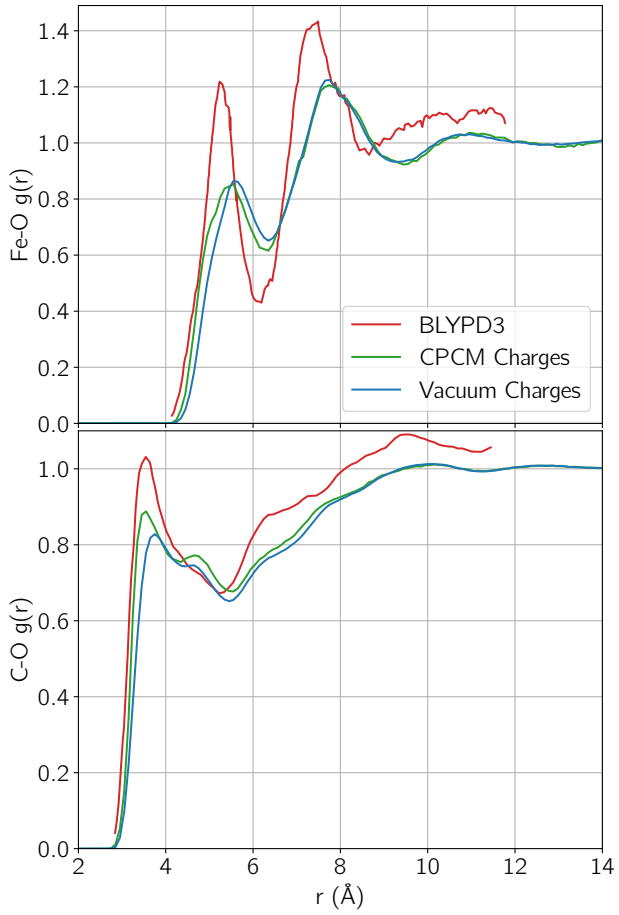

Figure S9: RDFs sampled from MD runs using the vacuum charges (blue curves) and the CPCM chargesr (green curves) from table S9, compared to the AIMD-sampled RDFs from literature[9,14] (red curves).

summed charge-differences on the ligands and the metal atom differ between the vacuum- and CPCM-derived partial charges. Therefore, the discrepancies between the DFT model and the MM model cannot simply be due to the pairwise additive Coulomb model being fed inaccurate partial charges.

We can also analyse the effect of the switching the partial charges on the shell-structures directly, by performing OPLS/TIP4PEW geometry-optimizations of the water-shells around the frozen B3LYP-D3(BJ) geometries of the complex (Geometries can be found in the next section). The average RMSD between vacuum and CPCM-relaxed water positions is 0.048 Å or roughly 15% of the RMSD between the B3LYP-D3(BJ)-relaxed geometries of the LS and

HS state. To see how this translates into liquid structure, figure S9 compares RDFs sampled from MD runs using the vacuum partial charges (blue curves) and CPCM partial charges (green curves). The CPCM-charges show slight improvements towards the AIMD results: both first peaks of Fe-O and C-O are shifted towards shorter distances, closer to the AIMD values. However, for the C-O RDF, the small peak around 5 Å, which isn't at all present in the AIMD curve, is amplified further. Lastly, especially for the Fe-O RDF, the differences brought about by switching the set of charges are much smaller than the differences between the AIMD and MM model.

Table S9: Partial atomic charges of $[Fe(bpy)_3]^{2+}$ from B3LYP-D3(BJ) calculations in vacuum and in the presence of CPCM implicit model of water solvent

Atom	CHELPG charges in vacuum			CHELPG charges in CPCM(water)		
	q(LS)	q(HS)	q(HS−LS)	q(LS)	q(HS)	q(HS−LS)
Fe	−0.635166	−0.167006	0.468160	−0.680959	−0.452249	0.228710
N	0.094239	−0.033615	−0.127854	0.105538	0.064529	−0.041009
C	−0.006578	0.053523	0.060101	−0.008469	−0.009065	−0.000596
H	0.088875	0.073423	−0.015452	0.110838	0.105067	−0.005771
C	−0.119239	−0.133335	−0.014096	−0.122253	−0.119674	0.002579
H	0.136129	0.135844	−0.000285	0.128467	0.124668	−0.003799
C	0.049594	0.057847	0.008253	0.032977	0.026492	−0.006485
H	0.122667	0.120053	−0.002614	0.114052	0.112517	−0.001535
C	−0.178988	−0.177662	0.001326	−0.177115	−0.170650	0.006465
H	0.145684	0.141051	−0.004633	0.147686	0.143520	−0.004166
C	0.103594	0.122880	0.019286	0.111678	0.103053	−0.008625
C	0.110394	0.122061	0.011667	0.118474	0.116526	−0.001948
C	−0.184813	−0.174041	0.010772	−0.182416	−0.178234	0.004182
H	0.147355	0.141176	−0.006179	0.149027	0.146069	−0.002958
C	0.052192	0.061295	0.009103	0.035064	0.042409	0.007345
H	0.122589	0.120868	−0.001721	0.114075	0.113628	−0.000447
C	−0.124264	−0.139273	−0.015009	−0.127705	−0.131671	−0.003966
H	0.137887	0.140131	0.002244	0.130352	0.128856	−0.001496
C	−0.003695	0.059587	0.063282	−0.003662	0.006367	0.010029
H	0.088162	0.070878	−0.017284	0.109067	0.105397	−0.003670
N	0.094317	−0.027581	−0.121898	0.104885	0.069429	−0.035456
N	0.101056	−0.029134	−0.130190	0.112973	0.058895	−0.054078
C	−0.009018	0.064656	0.073674	−0.011524	0.007293	0.018817
H	0.089382	0.068938	−0.020444	0.111926	0.106871	−0.005055
C	−0.120737	−0.143058	−0.022321	−0.123276	−0.126576	−0.003300
H	0.136900	0.139803	0.002903	0.129205	0.127772	−0.001433
C	0.051966	0.066866	0.014900	0.034775	0.049949	0.015174
H	0.122203	0.119634	−0.002569	0.113699	0.113557	−0.000142
C	−0.182606	−0.181971	0.000635	−0.179728	−0.181800	−0.002072
H	0.147017	0.143736	−0.003281	0.148699	0.147275	−0.001424
C	0.101125	0.129543	0.028418	0.108440	0.119207	0.010767
C	0.116420	0.111671	−0.004749	0.123935	0.133483	0.009548
C	−0.191202	−0.167207	0.023995	−0.188675	−0.190253	−0.001578
H	0.148647	0.137570	−0.011077	0.150403	0.148877	−0.001526
C	0.057464	0.052333	−0.005131	0.040104	0.054966	0.014862
H	0.121481	0.121447	−0.000034	0.112990	0.112892	−0.000098
C	−0.128179	−0.134805	−0.006626	−0.131057	−0.134004	−0.002947
H	0.138164	0.136985	−0.001179	0.130510	0.129035	−0.001475
C	0.001368	0.051119	0.049751	0.000091	0.018058	0.017967
H	0.086404	0.073717	−0.012687	0.108096	0.103291	−0.004805
N	0.090238	−0.027529	−0.117767	0.102520	0.049768	−0.052752
N	0.101218	−0.049938	−0.151156	0.111983	0.076293	−0.035690
C	−0.010729	0.068320	0.079049	−0.012124	−0.001969	0.010155

Table S9 – continued from previous page

H	0.089561	0.067305	−0.022256	0.111371	0.107547	−0.003824
C	−0.119069	−0.144140	−0.025071	−0.121680	−0.125630	−0.003950
H	0.136558	0.137901	0.001343	0.128927	0.127424	−0.001503
C	0.049626	0.061688	0.012062	0.032443	0.039742	0.007299
H	0.122390	0.118376	−0.004014	0.113808	0.113355	−0.000453
C	−0.177838	−0.174359	0.003479	−0.175120	−0.170905	0.004215
H	0.145223	0.139223	−0.006000	0.146816	0.143854	−0.002962
C	0.101742	0.122586	0.020844	0.109979	0.108103	−0.001876
C	0.104109	0.125506	0.021397	0.110742	0.101694	−0.009048
C	−0.181392	−0.177047	0.004345	−0.178587	−0.171886	0.006701
H	0.147310	0.140204	−0.007106	0.149163	0.144937	−0.004226
C	0.046714	0.064005	0.017291	0.029394	0.022616	−0.006778
H	0.123142	0.117788	−0.005354	0.114748	0.113223	−0.001525
C	−0.112090	−0.143542	−0.031452	−0.114867	−0.112046	0.002821
H	0.134039	0.137544	0.003505	0.126335	0.122484	−0.003851
C	−0.013690	0.068333	0.082023	−0.015809	−0.016870	−0.001061
H	0.090498	0.068871	−0.021627	0.112448	0.106727	−0.005721
N	0.103647	−0.051041	−0.154688	0.116323	0.075766	−0.040557

Sum	CHELPG charges in vacuum			CHELPG charges in CPCM(water)		
	q(LS)	q(HS)	q(HS−LS)	q(LS)	q(HS)	q(HS−LS)
Fe	−0.635166	−0.167006	0.468160	−0.680959	−0.452249	0.228710
Ligand 1	0.876101	0.735110	−0.140991	0.890560	0.799233	−0.091327
Ligand 2	0.878093	0.734314	−0.143779	0.894106	0.848556	−0.045550
Ligand 3	0.880969	0.697583	−0.183386	0.896293	0.804459	−0.091834

S5.5 Relationship between the 20-water cluster and the liquid-phase avg. shell

For completeness, we repeat the analysis of the 17-shell in the main text for the largest B3LYP-D3(BJ) optimized cluster in figure S10. The main change with respect to the 17-

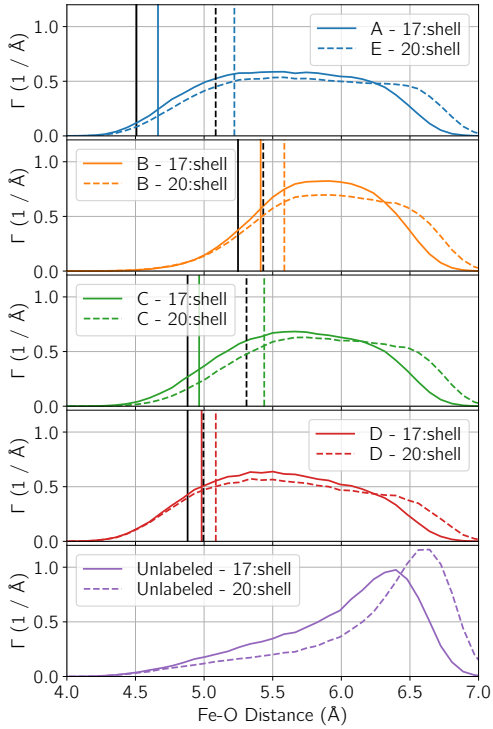

Figure S10: Histograms of the Fe-O distances of the 4 poses in the inner shell. The black lines represent the vacuum-optimized B3LYP-D3(BJ) distances, whereas the colored lines represent the vacuum-optimized OPLS/TIP4PEW distances, using the partial charges obtained from vacuum calculations. The "Unlabeled" distribution samples the Fe-O distances of OPLS/TIP4PEW poses that could not be unambiguously identified as one of the 4 poses from the B3LYP-D3(BJ) optimized shell, as the OPLS/TIP4PEW waters moved more than 3.4 Å to complete the linear sum assignment minimization with respect to the B3LYP-D3(BJ) optimized water positions.

water shell is that all poses shift slightly towards longer distances. This is because the B3LYP-D3(BJ) vacuum-distances have also all become longer, and thus the LSA-based labeling algorithm follows suit.

S5.6 LJ Parameters

Table S10: OPLS, CHARMM, and AMBER and Lennard-Jones parameters. The TIP4PEW LJ parameters are $\epsilon = 0.162750$ kcal/mol and $\sigma = 3.164350$ Å. It has no LJ parameters on its hydrogens. H' is the atom type of the H atoms on carbons adjacent to nitrogens in the bipyridine rings. For all simulations, the counterion Cl^- LJ parameters were $\epsilon = 0.6527$ kcal/mol and $\sigma = 4.13555$ Å, as assigned by the AMBER LEaP program.

Atom type	Fe	C	N	H	H'
			OPLS		
ϵ (kcal/mol)	0.013000	0.076000	0.170000	0.030000	N/A
σ (Å)	2.594000	3.550000	3.250000	2.420000	N/A
			CHARMM		
ϵ (kcal/mol)	0.000000	0.07000	0.060000	0.030000	0.046000
σ (Å)	1.158200	3.55005	3.367597	2.420037	1.959977
			AMBER		
ϵ (kcal/mol)	0.017200	0.08600	0.170000	0.015000	0.015000
σ (Å)	2.510560	3.39967	3.250000	2.599640	2.510550

S6 Further ΔV_{CS} and ΔV_{WW} Calculations

Table S11: Complex-Shell, Water-Water, and Total HS-LS differences in interaction energy of the 17-water shell. The leftmost column states which functional was used to optimize the geometries and calculate the interaction energy-differences.

Method	ΔV_{CS} (eV)	ΔV_{WW} (eV)	ΔV (eV)
B3LYP-D3(BJ)	-0.010	-0.151	-0.161
BLYP-D3(BJ)	-0.022	-0.163	-0.185
BLYP	-0.082	-0.136	-0.218

Table S11 compares the 17-Shell ΔV_{CS} and ΔV_{WW} values obtained from B3LYP-D3(BJ) with BLYP-D3(BJ). BLYP-D3(BJ) predicts stronger interactions for both terms, the complex-shell interaction is doubled, but due to its very small absolute size, the total change amounts to 0.024 eV, or 1.412 meV pr water molecule in the shell. Without dispersion correction, the BLYP results are weighed differently, with the complex-shell interaction increasing by roughly a factor of four, and the water-water interaction decreasing somewhat, amounting

to roughly twice as big differences between the D3- and non-D3 calculations as the differences from including exact exchange in calculations that both include long-range dispersion correction.

S6.1 BSSE Estimation of ΔV_{CS} and ΔV_{WW}

As mentioned in the computational details, we employed the "full" counterpoise-correction (CP), such that electron-less basis functions were placed on *all* nuclear positions of atoms that do not explicitly enter into the single-point calculation at hand.[15] I.e., if the subscript denominates the basis set used, and the parentheses contains the fragments ("C" = complex, "S" = water shell, "w_i" = water molecule i):

$$V_{\mathrm{CS}}^{\mathrm{CP}} = E_{\mathrm{CS}}(\mathrm{CS}) - E_{\mathrm{CS}}(\mathrm{CS}) - E_{\mathrm{CS}}(\mathrm{S}) \tag{1}$$

$$V_{\mathrm{WW}}^{\mathrm{CP}} = E_{\mathrm{CS}}(\mathrm{S}) - \sum_{i}^{N} E_{\mathrm{CS}}(\mathrm{w}_i), \tag{2}$$

where N is the number of water molecules in the shell. These values are used for the ΔV_{CS} and ΔV_{WW} in the main text. Table S12 shows both UC and CP-corrected energies calculated using B3LYP-D3(BJ)/def2-TZVP.

$$V_{\mathrm{CS}}^{\mathrm{UC}} = E_{\mathrm{CS}}(\mathrm{CS}) - E_{\mathrm{C}}(\mathrm{C}) - E_{\mathrm{S}}(\mathrm{S}) \tag{3}$$

$$V_{\mathrm{WW}}^{\mathrm{UC}} = E_{\mathrm{S}}(\mathrm{S}) - \sum_{i}^{N} E_{\mathrm{w}_i}(\mathrm{w}_i). \tag{4}$$

Table S12: Complex-Shell and Water-Water energies and BSSE-estimations in eV, obtained with B3LYP-D3(BJ)/def2-TZVP. The percentage is calculated with regards to the CP-corrected values. Since no CP-corrections can be carried out during sampling of molecular dynamics trajectories, the 11-16% overbinding in the terms could possibly cause some solvent-shell over-structuring, if this basis set were to be used.

		LS				HS			
n		UC	CP	BSSE	%	UC	CP	BSSE	%
17	V_{CS}	-3.298	-2.852	-0.446	16%	-3.306	-2.862	-0.444	16%
	V_{WW}	-5.888	-5.299	-0.589	11%	-6.056	-5.450	-0.606	11%
	V	-9.186	-8.151	-1.035	13%	-9.362	-8.312	-1.050	13%
18	V_{CS}	-3.545	-3.102	-0.443	14%	-3.542	-3.101	-0.441	14%
	V_{WW}	-6.484	-5.842	-0.642	11%	-6.603	-5.945	-0.658	11%
	V	-10.029	-8.945	-1.084	12%	-10.145	-9.046	-1.099	12%
19	V_{CS}	-3.750	-3.314	-0.436	13%	-3.729	-3.293	-0.436	13%
	V_{WW}	-6.972	-6.284	-0.688	11%	-7.083	-6.379	-0.704	11%
	V	-10.723	-9.598	-1.125	12%	-10.812	-9.672	-1.140	12%
20	V_{CS}	-3.905	-3.463	-0.442	13%	-3.911	-3.469	-0.442	13%
	V_{WW}	-7.495	-6.751	-0.744	11%	-7.561	-6.807	-0.754	11%
	V	-11.400	-10.214	-1.186	12%	-11.472	-10.277	-1.195	12%

S7 Further Many-Body Calculations

Table S13: Calculations of V_{2b} and V_{MB} on all possible combinations of spin configurations and optimized geometries. The percentage that the V_{MB} contribution make up of the total interaction energy V does not show the same increase to almost a fifth of the entire interaction energy when the calculation is carried out using the LS geometry in the HS spin configuration, instead of the HS geometry on the HS configuration. Calculating the V_{MB}-percentage in the LS configuration on the HS geometry gives a small increase.

	LS Configuration				HS Configuration			
	LS Geometry		HS Geometry		LS Geometry		HS Geometry	
	Energy (eV)	(%)	Energy (eV)	(%)	Energy (eV)	(%)	Energy (eV)	(%)
V_{2b}	-7.333	90	-7.332	87.8	-7.326	89.9	-6.753	81.2
V_{MB}	-0.818	10	-1.018	12.2	-0.823	10.1	-1.559	18.8
V	-8.151	100	-8.350	100	-8.150	100	-8.312	100

References

(1) Kühne, T. D. et al. CP2K: An electronic structure and molecular dynamics software package - Quickstep: Efficient and accurate electronic structure calculations. *J. Chem. Phys.* **2020**, *152*, 194103.

(2) Lippert, G.; Parrinello, M.; Hutter, J. A hybrid Gaussian and plane wave density functional scheme. *Mol. Phys.* **1997**, *92*, 477–488.

(3) VandeVondele, J.; Krack, M.; Mohamed, F.; Parrinello, M.; Chassaing, T.; Hutter, J. Quickstep: Fast and accurate density functional calculations using a mixed Gaussian and plane waves approach. *Comput. Phys. Commun.* **2005**, *167*, 103–128.

(4) Goedecker, S.; Teter, M.; Hutter, J. Separable dual-space Gaussian pseudopotentials. *Phys. Rev. B: Condens. Matter Mater. Phys.* **1996**, *54*, 1703.

(5) Hartwigsen, C.; Gœdecker, S.; Hutter, J. Relativistic separable dual-space Gaussian pseudopotentials from H to Rn. *Phys. Rev. B: Condens. Matter Mater. Phys.* **1998**, *58*, 3641.

(6) Krack, M. Pseudopotentials for H to Kr optimized for gradient-corrected exchange-correlation functionals. *Theor. Chem. Acc.* **2005**, *114*, 145–152.

(7) VandeVondele, J.; Hutter, J. Gaussian basis sets for accurate calculations on molecular systems in gas and condensed phases. *J. Chem. Phys.* **2007**, *127*, 114105.

(8) Martyna, G. J.; Tuckerman, M. E. A reciprocal space based method for treating long range interactions in ab initio and force-field-based calculations in clusters. *J. Chem. Phys.* **1999**, *110*, 2810–2821.

(9) Lawson Daku, L. Spin-state dependence of the structural and vibrational properties of solvated iron (ii) polypyridyl complexes from AIMD simulations: aqueous $[Fe(bpy)_3]Cl_2$, a case study. *Phys. Chem. Chem. Phys.* **2018**, *20*, 6236–6253.

(10) Li, P.; Merz, K. M. MCPB.py: A Python Based Metal Center Parameter Builder. *Journal of Chemical Information and Modeling* **2016**, *56*, 599–604.

(11) Miller, J. N.; McCusker, J. K. Outer-sphere effects on ligand-field excited-state dynamics: solvent dependence of high-spin to low-spin conversion in $[Fe(bpy)_3]^{2+}$. *Chemical Science* **2020**, *11*, 5191–5204.

(12) Skinner, L. B.; Benmore, C. J.; Neuefeind, J. C.; Parise, J. B. The structure of water around the compressibility minimum. *The Journal of Chemical Physics* **2014**, *141*, 214507.

(13) Ceriotti, M.; Fang, W.; Kusalik, P. G.; McKenzie, R. H.; Michaelides, A.; Morales, M. A.; Markland, T. E. Nuclear Quantum Effects in Water and Aqueous Systems: Experiment, Theory, and Current Challenges. *Chemical Reviews* **2016**, *116*, 7529–7550.

(14) Khakhulin, D.; Lawson Daku, L.; Leshchev, D.; Newby, G.; Jarenmark, M.; Bressler, C.; Wulff, M.; Canton, S. Visualizing the coordination-spheres of photoexcited transition metal complexes with ultrafast hard X-rays. *Phys. Chem. Chem. Phys.* **2019**, *21*, 9277–9284.

(15) Ouyang, J. F.; Cvitkovic, M. W.; Bettens, R. P. Trouble with the many-body expansion. *J. Chem. Theory Comput.* **2014**, *10*, 3699–3707.